Environmental Pollution 265 (2020) 115056

Contents lists available at ScienceDirect

Environmental Pollution

journal homepage: www.elsevier.com/locate/envpol

Persistent ozone pollution episodes in North China exacerbated by regional transport☆

Cheng Gong [a, b], Hong Liao [c, *], Lin Zhang [d], Xu Yue [c], Ruijun Dang [a, b], Yang Yang [c]

[a] State Key Laboratory of Atmospheric Boundary Layer Physics and Atmospheric Chemistry (LAPC), Institute of Atmospheric Physics, Chinese Academy of Sciences, Beijing, 100029, China
[b] University of Chinese Academy of Sciences, Beijing, 100049, China
[c] Jiangsu Key Laboratory of Atmospheric Environment Monitoring and Pollution Control, Jiangsu Collaborative Innovation Center of Atmospheric Environment and Equipment Technology, School of Environmental Science and Engineering, Nanjing University of Information Science and Technology, Nanjing, 210044, Jiangsu, China
[d] Laboratory for Climate and Ocean-Atmosphere Studies, Department of Atmospheric and Oceanic Sciences, School of Physics, Peking University, Beijing, 100871, China

ARTICLE INFO

Article history:
Received 8 April 2020
Received in revised form
31 May 2020
Accepted 16 June 2020
Available online 20 June 2020

Keywords:
Ozone pollution episode
North China
Regional transport
Cooperative emission reductions

ABSTRACT

Summertime ozone (O_3) concentrations over China continue to increase although the governmental Clear Air Actions have been carried out since 2013. The worst O_3 pollution is confronted over North China Plain. Ozone polluted days (with observed regionally-averaged maximum daily 8-h average (MDA8) O_3 concentrations exceeding 80 ppbv) in May–July in North China increased from 35 days in year 2014 to 56 days in year 2018, and persistent O_3 pollution episodes that lasted for 5 days or longer (OPEs5) contributed 14.3% and 66.1% to those O_3 polluted days in 2014 and 2018, respectively. Model simulations suggest that O_3 transport from central eastern China (including Shandong, Henan, Jiangsu and Anhui Provinces) contributes 36% of the enhanced O_3 concentrations in North China during OPEs5 relative to the seasonal mean. We find that emission control of volatile organic compounds in central eastern China is most effective to alleviate intensity of OPEs5 in North China.

1. Introduction

Surface ozone (O_3) is a major air pollutant generated by photochemical reactions of volatile organic compounds (VOCs) and nitrogen oxides (NO_x = NO + NO_2) (Sillman, 1999; Wang et al., 2006). A high level of surface O_3 is detrimental to both public health (Bell et al., 2006; Lelieveld et al., 2015; Nuvolone et al., 2018) and terrestrial vegetation (Ainsworth et al., 2012; Fuhrer et al., 1997; Yue et al., 2017). In addition, the intensification of O_3 enhances atmospheric oxidizing capacity and influences other chemical components in the troposphere (Atkinson, 2000; Kleinman et al., 2002).

Summertime O_3 concentrations have been increasing in eastern China (Dang and Liao, 2019; Li et al., 2019b; Liu et al., 2019; Lu et al., 2020; Wang et al., 2017b), which have become the top priorities for scientific research and control strategy (Li et al., 2019c) . North China (36.5°N-40.5°N, 114.5°E–119.5°E, green rectangle in Fig. 1a) has the highest O_3 levels in eastern China, with the observed maximum daily 8-h average (MDA8) O_3 concentrations reaching 60.1–90.6 ppbv as concentrations were averaged over summertime (May–July) of 2014–2018 (Fig. 1a). For individual observational sites in North China, the numbers of days with MDA8 O_3 concentrations exceeding 80 ppbv were very high (97–282 days) over the same time periods (Fig. 1b). The increases in O_3 concentration in eastern China were attributed in previous study to variations in meteorology as well as the control of particulate matter in recent years (Li et al., 2019b), because particulate matter scavenges the chemical radicals that would otherwise produce O_3 (Lou et al., 2014).

Accompanied with the high levels of summertime O_3 concentrations, the regional O_3 polluted days in North China tended to be consecutive and thus leading to more frequent and severe multi-day O_3 pollution episodes (OPEs) over the past several years (Gong and Liao, 2019). Here, OPEs in North China are defined as episodes during which the regionally-averaged daily MDA8 O_3 concentrations exceed 80 ppbv. We found OPEs with persistence of

☆ This paper has been recommended for acceptance by Pavlos Kassomenos

* Corresponding author.
E-mail address: hongliao@nuist.edu.cn (H. Liao).

https://doi.org/10.1016/j.envpol.2020.115056
0269-7491/

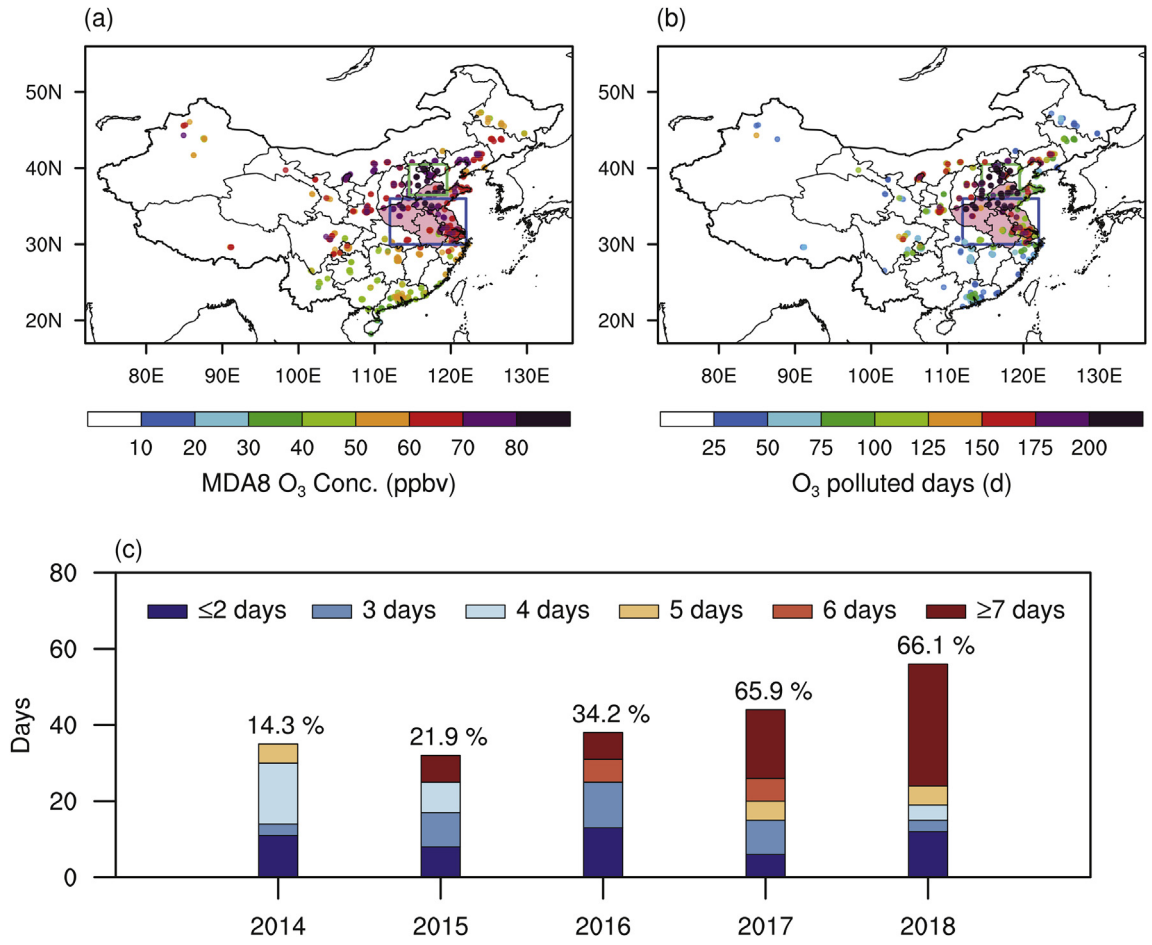

Fig. 1. Observed O_3 pollution over May to July in 2014–2018. (a). MDA8 O_3 concentrations (ppbv) averaged over May–July of 2014–2018 at the selected 729 observational sites operated by the China Ministry of Ecology and Environment. (b) The number of days with MDA8 O_3 concentrations exceeding 80 ppbv over May–July in 2014–2018. Green and blue rectangles indicate North China and central eastern China, respectively. Pink shade in (a) and (b) indicates the four provinces (Shandong, Henan, Jiangsu and Anhui) in central eastern China. (c) The number of days with observed regionally-averaged MDA8 O_3 concentration exceeding 80 ppbv in North China in May–July of 2014–2018. Different colors show the number of O_3 polluted days contributed from OPEs with different persistence. The percentage for each year indicates the ratio of days from OPEs5 (OPEs with persistence equal to or larger than 5 days) to the total regional O_3 polluted days in North China.

5 days or longer (OPEs5) contributed 14.3% of the 35 O_3 polluted days in 2014, and accounted for 66.1% of the 56 O_3 polluted days in 2018 (Fig. 1c). The occurrence of OPEs was highly associated with hot and dry weather conditions (Shu et al., 2016; Zhang et al., 2017). Previous studies have shown that high temperature could enhance the local O_3 chemical production (Pu et al., 2017; Schnell and Prather, 2017) while low humidity increased isoprene emissions from water-stressed plants (Zhang and Wang, 2016). Meanwhile, OPEs were found to be exacerbated by cross-city transport (Liu et al., 2019) as well as intercontinental transport (Pochanart et al., 2015; Zhang et al., 2009). However, few studies have systematically examined the role of regional transport (scale of hundreds of kilometers) of O_3 during OPEs in North China, especially this role in persistent episodes.

Central eastern China (30°N-36°N, 112°E–122°E, blue rectangle in Fig. 1a) is adjacent to North China and includes Shandong, Henan, Jiangsu and Anhui Provinces. Central eastern China also suffers from high levels of O_3 during summer (Fig. 1a and b) due to the high anthropogenic and biogenic emissions (Li et al., 2019a; Liu et al., 2018; Shu et al., 2020; Wang et al., 2017a). Meanwhile, southerlies prevail in eastern China during summer because of the East Asian summer monsoon (Yang et al., 2014), which are expected to transport air pollutants from central eastern China to North China. No previous studies have quantified the impact of such transport on multi-day OPEs in North China.

In this study, we examine persistent OPEs in North China represented by OPEs5. OPEs5 were selected considering both the longest persistence possible and the fact that the selected episode occurred at least once each year of 2014–2018 (Fig. 1c). We demonstrate first that O_3 transport from central eastern China influences OPEs5 in North China by analyses of composited wind fields and backward trajectories for OPEs5 as well as lead-time correlations of observed ground-level O_3 concentrations. Then the transport of O_3 from central eastern China to North China during OPEs5 is quantified by the tagged O_3 simulations with the Goddard Earth Observing System Chemical Transport Model (GEOS-Chem). Finally, model sensitivity experiments are carried out to highlight the importance of the cooperative emission control strategy for controlling OPEs5 in North China.

2. Data and methods

2.1. Ground-level O_3 observations

Hourly ground-level O_3 observations from May to July in 2014–2018 were obtained from the observational network of the

China Ministry of Ecology and Environment (http://datacenter.mee.gov.cn/websjzx/queryIndex.vm). The original unit of the observed O_3 concentrations is μg m^{-3}, which was converted to ppbv by utilizing the hourly values of SLP (surface level pressure) and 2-m temperature from the version 2 of Modern-Era Retrospective Analysis for Research and Application (MERRA2) reanalyzed data with the horizontal resolution of 0.5° × 0.625° (see below). An 8-h moving window for each day was applied to calculate the MDA8 O_3 concentration, and the window had to contain at least 6-h valid observations for calculating an 8-h average at each site. In addition, the monthly mean MDA8 O_3 concentration was calculated with at least 15 days of valid MDA8 values in each month. As a result, among the more than 1500 national sites, 729 sites were selected (Fig. S1), of which 61 sites are in North China and 145 sites are in central eastern China.

The diurnal variation of the hourly O_3 concentrations at each site was removed when calculating the lead time correlations:

$$[C_{d,h}] = \frac{C_{d,h} - \overline{C_h}}{s_h} \quad (1)$$

where $\overline{C_h}$ is the seasonal mean O_3 concentration at hour h averaged over May to July in 2014–2018 and s_h is the standard deviation of O_3 concentration at this site at hour h considering all days over May to July in 2014–2018. $C_{d,h}$ is the O_3 concentration at hour h on day d. $[C_{d,h}]$ indicates the hourly O_3 concentration with diurnal variation removed.

2.2. Reanalyzed meteorological dataset

The MERRA2 dataset was generated by NASA's Global Modeling and Assimilation Office by using the version 5 data assimilation system of the Goddard Earth Observing System (GEOS) Model and showed good consistency with observations at Chinese weather stations (Molod et al., 2015). The MERRA2 reanalyzed dataset we used has been modified by GEOS-Chem support team in the extended Asian domain (11°S-55°N, 60°E–150°E) with a horizontal resolution of 0.5° latitude x 0.667° longitude and 47 vertical layers up to 0.01 hPa (See details in http://wiki.seas.harvard.edu/geos-chem/index.php/MERRA-2). The surface and atmospheric meteorological parameters have temporal resolutions of 1 h and 3 h, respectively.

2.3. The HYSPLIT (hybrid single-particle Lagrangian integrated trajectory) model

The HYSPLIT version 4 (HYSPLIT-4) model was developed by the U.S. National Oceanic and Air Administration/Air Resources Laboratory (NOAA/ARL), which can compute simple air parcel trajectories and complex atmospheric dispersion (Draxier and Hess, 1998). Meteorological inputs to HYSPLIT-4 were from the National Centers for Environmental Prediction (NCEP) reanalysis with a horizontal resolution of 2.5° × 2.5° (http://ready.arl.noaa.gov/archives.php). Five-day backward trajectories were calculated four times a day (02:00, 08:00, 14:00, and 20:00 GMT+8) during the OPEs5 (91 days in total) started from 10 m height for two cities (Beijing (40°N, 116°E), the biggest city in North China, and Zibo (37°N, 118°E), the city with the highest seasonal-mean MDA8 O_3 concentrations of 90.6 ppbv over May to July in 2014–2018) in North China. Finally, a total of 364 trajectories were applied to obtain the clusters in the HYSPLIT cluster analysis, which was automatically implemented in HYSPLIT model by the variation of total spatial variance (TSV) with cluster numbers (See details in Liu et al. (2013)).

2.4. GEOS-chem model and the tagged O_3 technique

The GEOS-Chem model is a 3-D global chemical and transport model driven by MERRA2 reanalysis metrological data, which employs a fully coupled NO_x-O_x-hydrocarbon-aerosol chemistry mechanism to simulate concentrations of gas-phase pollutants (such as NO_x and O_3) and aerosols (including sulfate, nitrate, ammonium, organic carbon and black carbon, sea salt, and mineral dust) (Park et al., 2003; Pye et al., 2009). The model has 47 vertical layers up to 0.1 hPa level. The nested version of v11-01 in the Asian domain (11°S-55°N, 60°E–150°E) with a resolution of 0.5° latitude × 0.667° longitude was utilized in this study. Concentrations of all tracers at the lateral boundaries were provided by global simulations with a 2° latitude × 2.5° longitude horizontal resolution. The anthropogenic emissions were obtained from Multi-resolution Emission Inventory for China (MEIC, http://www.meicmodel.org) for years 2014–2017 (Li et al., 2017; Zheng et al., 2018). The emissions in 2018 were obtained by linear extrapolation of values over 2014–2017 for each grid. All simulations had a spin-up period of 6 months, and then results over May–July of 2014–2018 were analyzed.

The offline tagged O_3 simulation in the GEOS-Chem model has been widely used in previous studies (Han et al., 2018a; Ni et al., 2018; Whaley et al., 2015), which can quantify the contributions of O_3 from different regions to the daily mean O_3 concentrations in North China. Ten regions are considered, of which nine regions are in Asia and the last one represents the rest of the world (Fig. S2). Sum of these ten tagged O_3 concentrations in North China are in general equal to the simulated O_3 concentrations in this region. The 3-D O_3 production and loss rates were archived first in the full chemistry simulations and then utilized to tag O_3 geographically. O_3 generated from the surface to the 38th vertical layer in the model (about 50 hPa altitude) from the ten regions were all tagged. The tagged O_3 technique was applied in global simulations with a horizontal resolution of 2° × 2.5° and was driven by ozone production rates and loss frequencies archived from the standard simulation described above.

3. Results

3.1. Occurrence of OPEs5 over May–July of 2014–2018 in North China

Observations showed that 12 OPEs5 occurred in North China over May–July of 2014–2018 (Fig. 2). For these OPEs5, the averaged and maximum MDA8 O_3 concentrations were in the ranges of 91.4–115.3 ppbv and 102.4–133.7 ppbv, respectively (Table S1). Generally, OPEs5 became more frequent in recent years. There was only one episode in 2014 but 4 OPEs5 occurred in each of 2017 and 2018 (Fig. 2).

3.2. Evidences of O_3 transport from central eastern China to North China during OPEs5

Fig. 3a shows the composites of anomalous winds at 950 hPa (about 500 m altitude) for the 12 OPEs5 relative to the mean conditions of May–July in 2014–2018. Datasets of winds are from MERRA2 reanalyzed meteorological data. Strong anomalous southerlies prevailed in central eastern China, which could bring O_3 and its gaseous precursors from central eastern China to North China. Backward trajectories of the 12 OPEs5 for two typical cities (Beijing (40°N, 116°E) and Zibo (37°N, 118°E)) in North China, show that 53% and 72% of the trajectories originated from or passed through central eastern China (Fig. 3b and c), respectively. These trajectories are limited within 1000 m altitude (Fig. S3). Therefore,

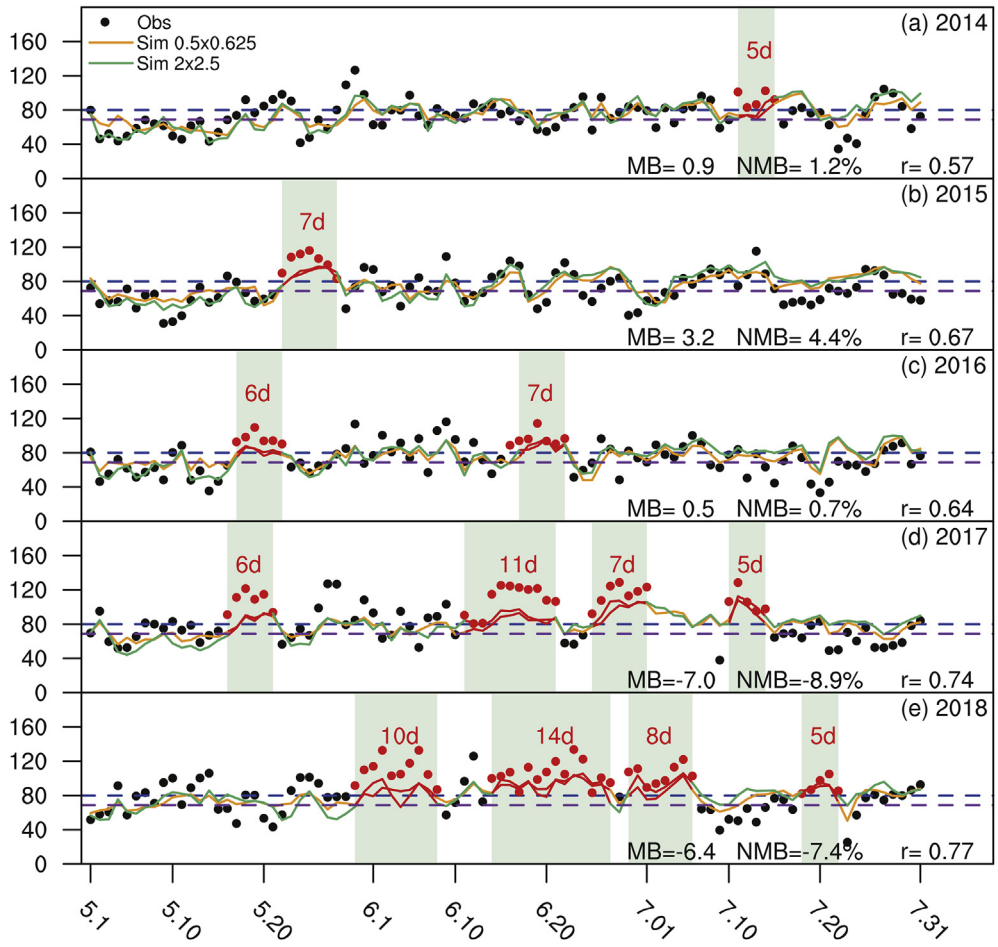

Fig. 2. Time series of the observed and simulated daily MDA8 O_3 concentrations in North China for May-July of 2014–2018. The black dots indicate the observed MDA8 O_3 concentration (ppbv) averaged over North China. The yellow and green lines indicate the GEOS-Chem simulated MDA8 O_3 concentrations averaged over North China with horizontal resolutions of 0.5° × 0.625° and 2° × 2.5°, respectively. Red dots indicate the observed OPEs5 in North China. Red numbers indicate the persistence of each observed OPE5. Red lines indicate the OPEs5 captured by the model, which are highlighted by the green shades. Correlation coefficient between the observed and simulated MDA8 O_3 concentrations for each year with a resolution of 0.5° × 0.625° is shown at the bottom right corner of each panel. The mean bias (MB) and normalized mean bias (NMB) are calculated by $MB = \frac{1}{n}\sum_i^n (S_i - O_i)$ and $NMB = \sum_i^n (S_i - O_i)/\sum_i^n O_i$*100%, respectively, where O_i and S_i indicate the observed and simulated MDA8 O_3 concentrations with a resolution of 0.5° × 0.625° on day i, respectively, and n indicates the total number of days.

O_3 in central eastern China is expected to influence the OPEs5 in North China through the regional transport.

Fig. 4 shows the lead-time correlations between the observed hourly O_3 concentrations averaged over North China during the 12 OPEs5 and the observed hourly O_3 concentrations at each site in China with the lead times of 0, 10, 20, 30, 40, and 50 h. The diurnal variations of O_3 concentrations at each site have been removed (eq. (1)). Interestingly, sites with strong positive correlations were found in the northern part of central eastern China (with the highest positive correlation coefficient of 0.75) when lead time of 20 h was applied to O_3 concentrations in central eastern China, and also in the YRD region when lead time of 30 h were considered (with highest positive correlation coefficient of 0.70). Meanwhile, the number of sites in central eastern China with statistically significant positive correlations increases from 39 (with lead time of 20 h) to 88 (with lead time of 30 h) and 73 (with lead time of 40 h) due to the denser observational sites in the YRD. The lead-time correlations further describe the transport pathway of O_3 polluted air mass by winds from central eastern China to North China during OPEs5.

3.3. Quantification of the O_3 transport during OPEs5 by the tagged O_3 technique

The GEOS-Chem model was utilized to quantify O_3 transport during OPEs5 in North China. Simulations generally captured the daily variations in MDA8 O_3 concentration, with the correlation coefficients between observations and model results in the range of 0.57–0.77 (Fig. 2). As for the identification of OPEs5 using the model results, we utilized a lower threshold of 68.8 ppbv (14.0% lower than 80 ppbv) in simulations, considering a normalized mean bias (NMB) of −14.0% when simulated MDA8 O_3 concentrations were compared with observations for days with observed MDA8 O_3 concentration larger than 80 ppbv. With the adjusted thresholds, all of the 12 OPEs5 were reproduced by the GEOS-Chem model (Fig. 2).

Table 1 shows the contributions of O_3 from different regions to surface O_3 in North China averaged over the 12 OPEs5 by applying the tagged O_3 technique. Locally generated O_3 (the 'North China' tagged O_3) contributes the largest fraction of O_3 in North China for either the OPEs5 or the mean conditions of May–July in 2014–2018. However, compared to the mean conditions, simulated daily mean O_3 concentrations in North China enhanced 11.1 ppbv

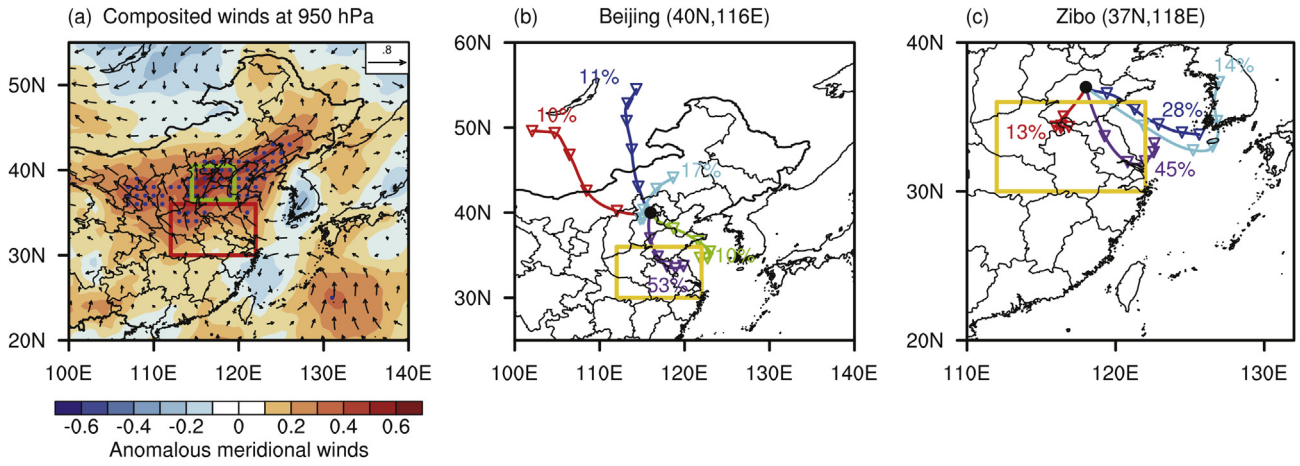

Fig. 3. Winds that transport O_3 from central eastern China to North China during OPEs5. (a) Composites of anomalous wind fields at 950 hPa during OPEs5 in North China relative to the seasonal-mean over May–July in 2014–2018. The daily time series of wind in each grid is standardized by the standard deviation. Shades indicate anomalous meridional wind speeds during OPEs5 relative to seasonal-mean. Blue dots indicate grids with statistically significant differences in meridional wind speed at 99% confidence level. The North China and central eastern China are enclosed by green and red rectangles, respectively. (b)–(c) Five-day backward trajectories of the air mass at two cities (Beijing and Zibo) in North China for days of OPEs5 over May–July in 2014–2018. The trajectories are retrieved at 2:00, 8:00, 14:00 and 20:00 GMT +8 for each day during the OPEs5. Inverted triangles appear every 24 h on each trajectory. The percentages with different colors indicate the frequencies of different trajectories. The yellow rectangle encloses central eastern China.

during the OPEs5, of which O_3 from North China and central eastern China contribute 7.3 ppbv and 4.0 ppbv, respectively. O_3 from other regions show neglectable changes of <0.4 ppbv from mean conditions to OPEs5. These results indicate that O_3 transport from central eastern China contributed, on average, 36.0% to the increased O_3 concentration in North China during the OPEs5.

3.4. *Emission reduction in central eastern China alleviates OPEs5 in North China*

Four sensitivity experiments were performed with 50% reductions in anthropogenic emissions of either NO_x or VOCs over North China or central eastern China to examine the effectiveness of short-term emission control on the intensity of OPEs5. For each OPE5, the emission reduction was executed from one day before the OPE5 to the last day of the episode. Fig. 5 shows that the averaged MDA8 O_3 concentrations in North China decrease by 1.5 ppbv and 3.3 ppbv with the 50% local emission reductions in NO_x and VOCs, respectively, indicating that local reduction in VOCs is more helpful to weaken O_3 pollution. Surprisingly, emission reductions in central eastern China are more effective than those local reductions in terms of alleviating the intensity of OPEs5 in North China. The averaged MDA8 O_3 concentrations during OPEs5 in North China decrease by 1.9 ppbv and 4.0 ppbv when 50% reductions in NO_x and VOCs are carried out in central eastern China alone. This suggests that performing regional cooperative emission control is necessary and important to alleviate the intensity of OPEs5 in North China.

We further examine the impacts on MDA8 O_3 concentrations in North China for each day of the 12 OPEs5 when emission reductions are carried out. Previous studies have shown that O_3 formation in megacities (such as Beijing-Tianjin-Hebei and YRD regions) was generally VOCs-limited (Han et al., 2018b; Wang et al., 2019b; Wang et al., 2017a), while O_3 formation in most suburban and rural regions over eastern China exhibited mixed NO_x-VOCs sensitivity (Wang et al., 2019a). As a result, Fig. S4 showed reductions in NO_x can either increase or reduce regionally-averaged MDA8 O_3 concentrations in North China (ranging from −7.3 to 3.6 ppbv for reduction in North China and from −8.2 to 1.3 ppbv for reduction in central eastern China) depending on the ratios of NO_x/VOCs, while emission controls on VOCs generally reduce O_3 concentrations (ranging from −8.3 to −0.4 ppbv for reduction in North China and −10.1 to 0.1 ppbv for reduction in central eastern China). By examining the relationships between the daily mean southerlies at 950 hPa averaged over the south border of North China (36.5°N, 114.5°-119.5°E) and the reductions in daily MDA8 O_3 concentrations averaged over North China for the 12 OPEs5, we find that the MDA8 O_3 concentrations in North China can be reduced most efficiently under the conditions of strong southerlies as the emission reductions are carried out in central eastern China. When wind speed of southerlies exceeds 4 m s^{-1}, highest reductions in MDA8 O_3 concentrations in North China occur, reaching 1.8–3.4 ppbv and 4.0–5.6 ppbv with 50% reductions in NO_x and VOCs in central eastern China, respectively (Fig. S5a). However, such relationship between southerlies and MDA8 O_3 in North China is not found in the case of local emission control. As a result, emission control in central eastern China is more effective to reduce the peak O_3 concentrations of OPEs5 in North China (Fig. S6). This conclusion agrees with the fact that the observed MDA8 O_3 concentrations over North China were the highest (exceeded 100 ppbv) when southerlies had wind speed of larger than 4 m s^{-1} (Fig. S5b).

4. Discussions

In this study, we highlight the importance of O_3 transport from central eastern China to the OPEs5 in North China. However, precisely quantifying the magnitude of the regional transport is still a challenge. The transport of O_3 precursors have been shown to have large influence on O_3 concentrations in downwind regions (Han et al., 2018b; Liu et al., 2020), but the tagged O_3 technique accounts for only the transport of O_3 (Ni et al., 2018; Whaley et al., 2015). As a result, the contributions of regional transport to OPEs5 in North China obtained in this study might be underestimated, considering O_3 generated from precursors from central eastern China was tagged as local O_3 in North China.

The occurrences of muti-day O_3 pollution episodes in North China are also associated with the high levels of seasonal-mean O_3 concentrations. To alleviate the muti-day O_3 pollution episodes, on the one hand, strategies for reducing anthropogenic emissions of NO_x and VOCs should be executed strictly (Li et al., 2019c) to reduce the total amount of O_3 production during summer. On the other

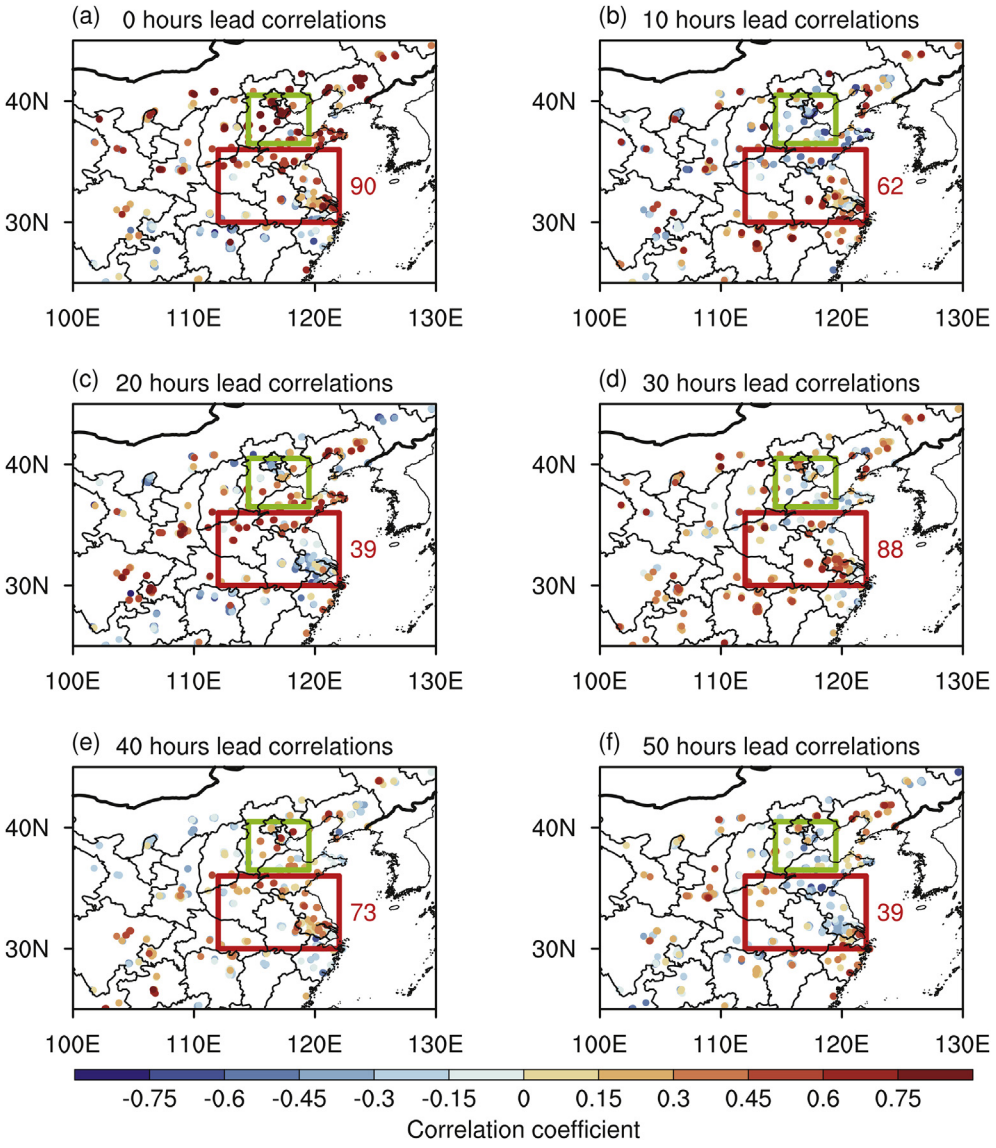

Fig. 4. Lead-time correlations between the observed hourly O_3 concentrations averaged over North China during the 12 OPEs5 (91 days in total) and the observed hourly O_3 concentrations at each site in China. The diurnal variation in hourly O_3 concentrations at each site is removed by utilizing eq. (1). The lead time is from 0 to 50 h. All the sites shown in the panels have statistically significant lead-time correlation coefficients at the 99% confidence level. Red numbers indicate the number of sites in central eastern China with statistically significant positive correlations. The green and red rectangles indicate North China and central eastern China, respectively.

Table 1
Tagged surface O_3 concentrations in North China from ten regions.

	Sum	North China	Northeast	South	Southeast ocean	North	Southwest	Central eastern China	Tibet	North west	Rest of world
OPEs5[a] (ppbv)	71.1	54.5	2.4	0.02	0.07	0.7	0.04	9.3	0.01	3.8	0.3
Mean[b] (ppbv)	60.0	47.2	2.5	0.02	0.08	0.9	0.03	5.3	0.01	3.4	0.5
Differences (ppbv)	11.1	7.3	−0.1	0	−0.01	−0.2	0.01	4.0	0	0.4	−0.3

[a] Averaged over the 12 OPEs5 in North China.
[b] Averagerd over May–July of years 2014–2018.

hand, the favorable weather conditions should also be emphasized (Gong and Liao, 2019; Yin et al., 2019) with corresponding short-term emission control. Reducing emissions in upwind region has been proved to be effective in alleviating $PM_{2.5}$ episodes (Hua et al., 2016; Li et al., 2018; Wang et al., 2014). Our results highlight that the cooperative regional emission control in central eastern China would have a better effect than considering local control only for the muti-day O_3 pollution episodes in North China.

Over 2014–2018, in North China and central eastern China, NO_x emissions decreased but VOCs emissions increased (Fig. S7). The increase in VOCs may offset the benefit contributed by NO_x reduction. Meanwhile, O_3 concentrations in central eastern China were observed to have an increasing trend in terms of either seasonal mean concentrations of MDA8 or the averaged MDA8 O_3 concentrations during the OPEs5 (Fig. S8). If the increasing trend continues, the potential risks of severe O_3 episode in North China

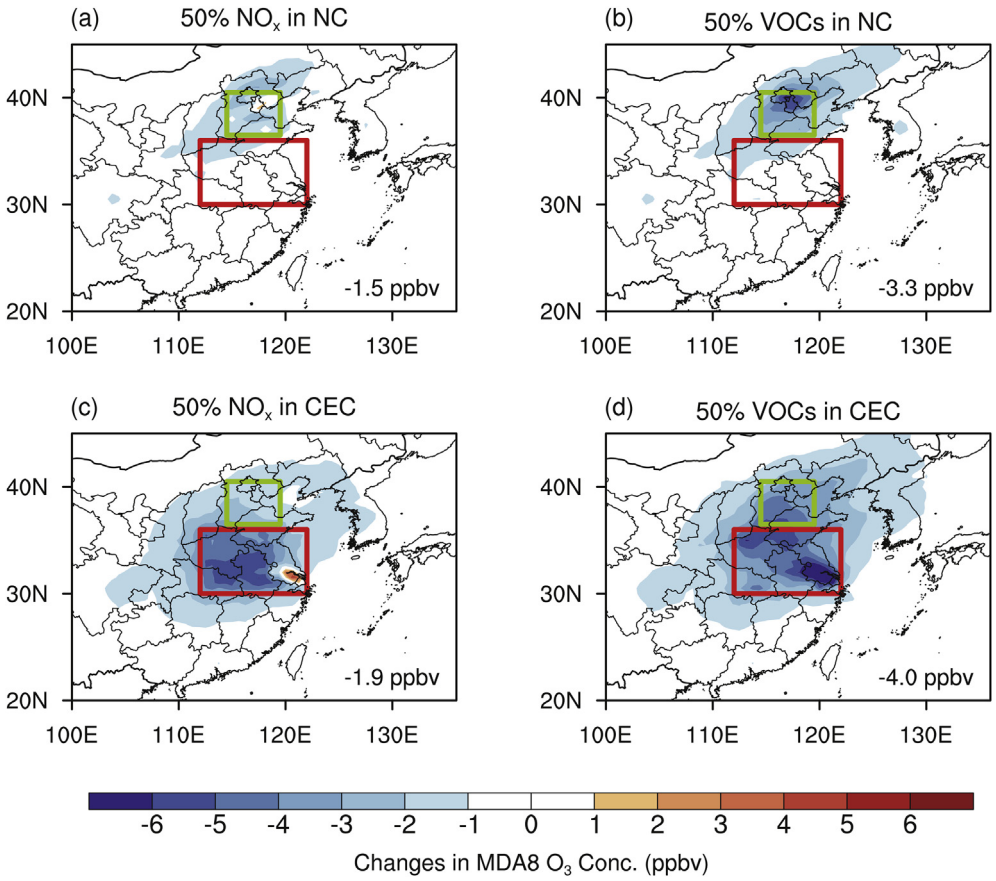

Fig. 5. Changes in MDA8 O_3 concentration (ppbv) averaged over 12 OPEs5 as a result of emission reductions. Changes induced by (a) 50% reduction in NO_x emissions in North China, (b) 50% reduction in VOCs emissions in North China, (c) 50% reduction in NO_x emissions in central eastern China, and (d) 50% reduction in VOCs emissions in central eastern China. The emission reductions are all carried out in the GEOS-Chem model from one day before each OPE5 to the end of each OPE.

would become higher considering the transport mechanism.

5. Conclusion

In summary, persistent O_3 pollution episodes were observed to increase in North China. In this study, the composited wind fields and backward trajectories, lead-time correlation of the observations, as well as the GEOS-Chem model simulations were utilized together to verify the important contributions of O_3 transport from central eastern China to OPEs5 in North China. By applying the tagged O_3 technique in GEOS-Chem model, we found that O_3 transport from central eastern China contributed on average 36.0% to the increased O_3 concentration in North China during the OPEs5. Sensitivity experiments reveal that short-term emissions reduction is effective to alleviate OPEs5 in North China. Reductions in VOCs (NO_x) by 50% in central eastern China can reduce the MDA8 O_3 concentrations averaged over North China by 4.0 (1.9) ppbv during the OPEs5, which is more efficient than the reduction in MDA8 O_3 of 3.3 (1.5) ppbv resulted from the 50% reduction in VOCs (NO_x) in North China. Our results highlight the importance of cooperative regional emission control to alleviate severe O_3 pollution episodes in North China.

CRediT authorship contribution statement

Cheng Gong: Conceptualization, Methodology, Software, Validation, Formal analysis, Investigation, Writing - original draft, Visualization. **Hong Liao:** Conceptualization, Validation, Writing - review & editing, Supervision, Project administration, Funding acquisition. **Lin Zhang:** Validation, Writing - review & editing. **Xu Yue:** Validation, Writing - review & editing. **Ruijun Dang:** Resources. **Yang Yang:** Writing - review & editing.

Declaration of competing interest

The authors declare no competing financial interests.

Acknowledgement

This work was supported by the National Natural Science Foundation of China (grant no. 91744311), the National Key Research and Development Program of China (grant no. 2019YFA0606804), and the Major Research Plan of the National Social Science Foundation (grant no. 18ZDA052).

Appendix A. Supplementary data

Supplementary data to this article can be found online at https://doi.org/10.1016/j.envpol.2020.115056.

References

Ainsworth, E.A., Yendrek, C.R., Sitch, S., Collins, W.J., Emberson, L.D., 2012. The effects of tropospheric ozone on net primary productivity and implications for climate change. In: Merchant, S.S. (Ed.), Annu. Rev. Plant. Biol, vol. 63, pp. 637–661.
Atkinson, R., 2000. Atmospheric chemistry of VOCs and NOx. Atmos. Environ. 34, 2063–2101.

Bell, M.L., Peng, R.D., Dominici, F., 2006. The exposure-response curve for ozone and risk of mortality and the adequacy of current ozone regulations. Environ. Health Perspect. 114, 532–536.
Dang, R., Liao, H., 2019. Radiative forcing and health impact of aerosols and ozone in China as the consequence of clean air actions over 2012-2017. Geophys. Res. Lett. 46, 12511–12519.
Draxier, R.R., Hess, G.D., 1998. An overview of the HYSPLIT_4 modelling system for trajectories, dispersion and deposition. Aust. Meteorol. Mag. 47, 295–308.
Fuhrer, J., Skarby, L., Ashmore, M.R., 1997. Critical levels for ozone effects on vegetation in Europe. Environ. Pollut. 97, 91–106.
Gong, C., Liao, H., 2019. A typical weather pattern for ozone pollution events in North China. Atmos. Chem. Phys. 19, 13725–13740.
Han, H., Liu, J., Yuan, H., Zhuang, B., Zhu, Y., Wu, Y., Yan, Y., Ding, A., 2018a. Characteristics of intercontinental transport of tropospheric ozone from Africa to Asia. Atmos. Chem. Phys. 18, 4251–4276.
Han, X., Zhu, L., Wang, S., Meng, X., Zhang, M., Hu, J., 2018b. Modeling study of impacts on surface ozone of regional transport and emissions reductions over North China Plain in summer 2015. Atmos. Chem. Phys. 18, 12207–12221.
Hua, Y., Wang, S., Wang, J., Jiang, J., Zhang, T., Song, Y., Kang, L., Zhou, W., Cai, R., Wu, D., Fan, S., Wang, T., Tang, X., Wei, Q., Sun, F., Xiao, Z., 2016. Investigating the impact of regional transport on PM2.5 formation using vertical observation during APEC 2014 Summit in Beijing. Atmos. Chem. Phys. 16, 15451–15460.
Kleinman, L.I., Daum, P.H., Lee, Y.N., Nunnermacker, L.J., Springston, S.R., Weinstein-Lloyd, J., Rudolph, J., 2002. Ozone production efficiency in an urban area. J. Geophys. Res. Atmos. 107.
Lelieveld, J., Evans, J.S., Fnais, M., Giannadaki, D., Pozzer, A., 2015. The contribution of outdoor air pollution sources to premature mortality on a global scale. Nature 525, 367-+.
Li, B., Ho, S.S.H., Gong, S., Ni, J., Li, H., Han, L., Yang, Y., Qi, Y., Zhao, D., 2019a. Characterization of VOCs and their related atmospheric processes in a central Chinese city during severe ozone pollution periods. Atmos. Chem. Phys. 19, 617–638.
Li, K., Jacob, D.J., Liao, H., Shen, L., Zhang, Q., Bates, K.H., 2019b. Anthropogenic drivers of 2013-2017 trends in summer surface ozone in China. P. Natl. Acad. Sci. Usa. 116, 422–427.
Li, K., Jacob, D.J., Liao, H., Zhu, J., Shah, V., Shen, L., Bates, K.H., Zhang, Q., Zhai, S., 2019c. A two-pollutant strategy for improving ozone and particulate air quality in China. Nat. Geosci. 12, 906-+.
Li, M., Zhang, Q., Kurokawa, J.-i., Woo, J.-H., He, K., Lu, Z., Ohara, T., Song, Y., Streets, D.G., Carmichael, G.R., Cheng, Y., Hong, C., Huo, H., Jiang, X., Kang, S., Liu, F., Su, H., Zheng, B., 2017. MIX: a mosaic Asian anthropogenic emission inventory under the international collaboration framework of the MICS-Asia and HTAP. Atmos. Chem. Phys. 17, 935–963.
Li, N., Lu, Y., Liao, H., He, Q., Li, J., Long, X., 2018. WRF-Chem modeling of particulate matter in the Yangtze River Delta region: source apportionment and its sensitivity to emission changes. PloS One 13.
Liu, H., Zhang, M., Han, X., Li, J., Chen, L., 2019. Episode analysis of regional contributions to tropospheric ozone in Beijing using a regional air quality model. Atmos. Environ. 199, 299–312.
Liu, J., Wang, L., Li, M., Liao, Z., Sun, Y., Song, T., Gao, W., Wang, Y., Li, Y., Ji, D., Hu, B., Kerminen, V.-M., Wang, Y., Kulmala, M., 2019. Quantifying the impact of synoptic circulation patterns on ozone variability in northern China from April to October 2013-2017. Atmos. Chem. Phys. 19, 14477–14492.
Liu, N., Yu, Y., He, J., Zhao, S., 2013. Integrated modeling of urban-scale pollutant transport: application in a semi-arid urban valley, Northwestern China. Atmos. Pollut. Res. 4, 306–314.
Liu, Y., Li, L., An, J., Huang, L., Yan, R., Huang, C., Wang, H., Wang, Q., Wang, M., Zhang, W., 2018. Estimation of biogenic VOC emissions and its impact on ozone formation over the Yangtze River Delta region, China. Atmos. Environ. 186, 113–128.
Liu, Y., Song, M., Liu, X., Zhang, Y., Hui, L., Kong, L., Zhang, Y., Zhang, C., Qu, Y., An, J., Ma, D., Tan, Q., Feng, M., 2020. Characterization and sources of volatile organic compounds (VOCs) and their related changes during ozone pollution days in 2016 in Beijing, China. Environ. Pollut. 257.
Lou, S., Liao, H., Zhu, B., 2014. Impacts of aerosols on surface-layer ozone concentrations in China through heterogeneous reactions and changes in photolysis rates. Atmos. Environ. 85, 123–138.
Lu, X., Zhang, L., Wang, X., Gao, M., Li, K., Zhang, Y., Yue, X., Zhang, Y., 2020. Rapid Increases in Warm-Season Surface Ozone and Resulting Health Impact in China Since 2013.Environ. Sci. Technol. Lett. 7, 240–247.
Molod, A., Takacs, L., Suarez, M., Bacmeister, J., 2015. Development of the GEOS-5 atmospheric general circulation model: evolution from MERRA to MERRA2. Geosci. Model Dev. (GMD) 8, 1339–1356.
Ni, R., Lin, J., Yan, Y., Lin, W., 2018. Foreign and domestic contributions to springtime ozone over China. Atmos. Chem. Phys. 18, 11447–11469.
Nuvolone, D., Petri, D., Voller, F., 2018. The effects of ozone on human health. Environ. Sci. Pollut. Res. 25, 8074–8088.
Park, R.J., Jacob, D.J., Chin, M., Martin, R.V., 2003. Sources of carbonaceous aerosols over the United States and implications for natural visibility. J. Geophys. Res. Atmos. 108.
Pochanart, P., Wang, Z., Akimoto, H., 2015. Boundary layer ozone transport from eastern China to southern Japan: pollution episodes observed during monsoon onset in 2004. Asian J. Atmospheric Environ. 9, 48–56.
Pu, X., Wang, T.J., Huang, X., Melas, D., Zanis, P., Papanastasiou, D.K., Poupkou, A., 2017. Enhanced surface ozone during the heat wave of 2013 in Yangtze River Delta region, China. Sci. Total Environ. 603–604, 807–816.
Pye, H.O.T., Liao, H., Wu, S., Mickley, L.J., Jacob, D.J., Henze, D.K., Seinfeld, J.H., 2009. Effect of changes in climate and emissions on future sulfate-nitrate-ammonium aerosol levels in the United States. J. Geophys. Res. Atmos. 114.
Schnell, J.L., Prather, M.J., 2017. Co-occurrence of extremes in surface ozone, particulate matter, and temperature over eastern North America. Proc. Natl. Acad. Sci. U. S. A. 114, 2854–2859.
Shu, L., Wang, T., Han, H., Xie, M., Chen, P., Li, M., Wu, H., 2020. Summertime ozone pollution in the Yangtze River Delta of eastern China during 2013-2017: synoptic impacts and source apportionment. Environ. Pollut. 257.
Shu, L., Xie, M., Wang, T., Gao, D., Chen, P., Han, Y., Li, S., Zhuang, B., Li, M., 2016. Integrated studies of a regional ozone pollution synthetically affected by subtropical high and typhoon system in the Yangtze River Delta region, China. Atmos. Chem. Phys. 16, 15801–15819.
Sillman, S., 1999. The relation between ozone, NOx and hydrocarbons in urban and polluted rural environments. Atmos. Environ. 33, 1821–1845.
Wang, N., Lyu, X.P., Deng, X.J., Huang, X., Jiang, F., Ding, A.J., 2019a. Aggravating O-3 pollution due to NOx emission control in eastern China. Sci. Total Environ. 677, 732–744.
Wang, P., Chen, Y., Hu, J., Zhang, H., Ying, Q., 2019b. Attribution of tropospheric ozone to NOx and VOC emissions: considering ozone formation in the transition regime. Environ. Sci. Technol. 53, 1404–1412.
Wang, T., Xue, L., Brimblecombe, P., Lam, Y.F., Li, L., Zhang, L., 2017a. Ozone pollution in China: a review of concentrations, meteorological influences, chemical precursors, and effects. Sci. Total Environ. 575, 1582–1596.
Wang, T.J., Lam, K.S., Xie, M., Wang, X.M., Carmichael, G., Li, Y.S., 2006. Integrated studies of a photochemical smog episode in Hong Kong and regional transport in the Pearl River Delta of China. Tellus B 58, 31–40.
Wang, W.N., Cheng, T.H., Gu, X.F., Chen, H., Guo, H., Wang, Y., Bao, F.W., Shi, S.Y., Xu, B.R., Zuo, X., Meng, C., Zhang, X.C., 2017b. Assessing spatial and temporal patterns of observed ground-level ozone in China. Sci. Rep. 7, 3651.
Wang, Z., Li, J., Wang, Z., Yang, W., Tang, X., Ge, B., Yan, P., Zhu, L., Chen, X., Chen, H., Wand, W., Li, J., Liu, B., Wang, X., Wand, W., Zhao, Y., Lu, N., Su, D., 2014. Modeling study of regional severe hazes over mid-eastern China. in January 2013 and its implications on pollution prevention and control. Sci. China Earth Sci 57, 3–13.
Whaley, C.H., Strong, K., Jones, D.B.A., Walker, T.W., Jiang, Z., Henze, D.K., Cooke, M.A., McLinden, C.A., Mittermeier, R.L., Pommier, M., Fogal, P.F., 2015. Toronto area ozone: long-term measurements and modeled sources of poor air quality events. J. Geophys. Res. Atmos. 120, 11368–11390.
Yang, Y., Liao, H., Li, J., 2014. Impacts of the East Asian summer monsoon on interannual variations of summertime surface-layer ozone concentrations over China. Atmos. Chem. Phys. 14, 6867–6879.
Yin, Z., Cao, B., Wang, H., 2019. Dominant patterns of summer ozone pollution in eastern China and associated atmospheric circulations. Atmos. Chem. Phys. 19, 13933–13943.
Yue, X., Unger, N., Harper, K., Xia, X., Liao, H., Zhu, T., Xiao, J., Feng, Z., Li, J., 2017. Ozone and haze pollution weakens net primary productivity in China. Atmos. Chem. Phys. 17, 6073–6089.
Zhang, H., Wang, Y., Park, T.-W., Deng, Y., 2017. Quantifying the relationship between extreme air pollution events and extreme weather events. Atmos. Res. 188, 64–79.
Zhang, L., Jacob, D.J., Kopacz, M., Henze, D.K., Singh, K., Jaffe, D.A., 2009. Intercontinental source attribution of ozone pollution at western US sites using an adjoint method. Geophys. Res. Lett. 36.
Zhang, Y., Wang, Y., 2016. Climate-driven ground-level ozone extreme in the fall over the Southeast United States. Proc. Natl. Acad. Sci. U. S. A. 113, 10025–10030.
Zheng, B., Tong, D., Li, M., Liu, F., Hong, C., Geng, G., Li, H., Li, X., Peng, L., Qi, J., Yan, L., Zhang, Y., Zhao, H., Zheng, Y., He, K., Zhang, Q., 2018. Trends in China's anthropogenic emissions since 2010 as the consequence of clean air actions. Atmos. Chem. Phys. 18, 14095–14111.